

# A DIRECT APPROACH TO FINDING UNKNOWN BOUNDARY CONDITIONS IN STEADY HEAT CONDUCTION

Thomas J. Martin\* and George S. Dulikravich\*\*  
Department of Aerospace Engineering  
The Pennsylvania State University, University Park, PA 16802, USA

## SUMMARY

The capability of the boundary element method (BEM) in determining thermal boundary conditions on surfaces of a conducting solid where such quantities are unknown has been demonstrated. The method uses a non-iterative direct approach in solving what is usually called the inverse heat conduction problem (IHCP). Given any over-specified thermal boundary conditions such as a combination of temperature and heat flux on a surface where such data is readily available, the algorithm computes the temperature field within the object and any unknown thermal boundary conditions on surfaces where thermal boundary values are unavailable. A two-dimensional, steady-state BEM program has been developed and was tested on several simple geometries where the analytic solution was known. Results obtained with the BEM were in excellent agreement with the analytic values. The algorithm is highly flexible in treating complex geometries, mixed thermal boundary conditions and temperature-dependent material properties and is presently being extended to three-dimensional and unsteady heat conduction problems. The accuracy and reliability of this technique was very good but tended to deteriorate when the known surface conditions were only slightly over-specified and far from the inaccessible surface.

## INTRODUCTION

The objective of the steady-state inverse heat conduction problem is to deduce temperatures and heat fluxes on any surface or surface element where such information is unknown. In many instances it is impossible to place sensors and take measurements on a particular surface of a conducting solid due to the inaccessibility or severity of the environment on that surface. These unknown thermal boundary values may be deduced from additional temperature or heat flux measurements made within the solid or on some other surface of the solid. This problem has been given a considerable amount of attention by a variety of researchers and virtually all work has been directed to the one-dimensional transient problem. The first method proposed to solve the IHCP used inversion of convolution integrals (Stolz 1960) and was subsequently improved by a number of authors (Beck et al. 1988). Many other methods have also been developed using such techniques as Laplace transforms, finite elements, time-marching finite differences and other approaches. A detailed chronological review of the IHCP literature has been provided by Hensel (1992).

A characteristic of most of these inverse techniques is that they tend to produce temporal oscillations in the unknown surface thermal condition estimates that are larger than the temporal oscillations in the over-specified thermal data as it propagates through the solid (Hills and Hensel 1986). In other words, the random noise due to round off errors tends to magnify as the solution proceeds and quickly produces a useless solution, especially as the distance between the surface and the over-specified information increases. A number of authors have presented various smoothing techniques for reducing this error growth, but the effect of these operations on the accuracy of the solution is not easy to evaluate (Murio 1993).

---

\* Graduate research assistant.

\*\* Associate professor.

The method presented herein does not utilize any artificial smoothing technique and is not limited to transient or one-dimensional problems. This approach is non-iterative and has been shown to compute meaningful and accurate thermal fields in a single analysis using a straightforward modification to the boundary element method (BEM).

The BEM is a very accurate and efficient technique that can solve boundary value problems such as those governing heat conduction, electromagnetic fields, irrotational incompressible fluid flow, elasticity and many other physical phenomenon. For steady-state heat conduction analysis using the BEM, either temperatures,  $T$ , or heat fluxes,  $Q$ , are specified everywhere on the surface of the solid where one of these quantities is known while the other is unknown. In the BEM solution to the IHCP, both  $T$  and  $Q$  must be specified on a part of the solid's surface, while both  $T$  and  $Q$  are unknown on another part of the surface. Elsewhere on the solid's surface, normal boundary conditions should be applied as either  $T$ 's or  $Q$ 's. The surface section where both  $T$  and  $Q$  are specified simultaneously is called the over-specified boundary and is necessary for the IHCP problem's solution.

Figure 1 illustrates a typical two-dimensional, multiply connected, inverse heat conduction problem. Surfaces labeled  $\Gamma_1$  are the over-specified boundaries where both  $T$  and  $Q$  are given. Normal boundary conditions (either  $T$  or  $Q$  specified) are enforced on the surfaces labeled  $\Gamma_2$ . Thermal data is assumed to be inaccessible on the inner  $\Gamma_3$  surface and thus has both  $T$  and  $Q$  unknown on this boundary. The objective of the IHCP is to compute temperatures and heat fluxes on the boundary  $\Gamma_3$  using only the values of  $T$  and  $Q$  provided on the surface of the solid and, possibly, additional temperature measurements made within the solid if such data is available.

## THEORY

### Two-Dimensional Steady-State BEM

Steady-state heat conduction in a homogeneous medium with a constant coefficient of thermal conductivity is governed by the Laplace's equation in the region,  $\Omega$ , of a conducting solid

$$\nabla^2 T = 0 \quad (1)$$

where  $T$  is the temperature. This is a linear boundary value problem having essential boundary conditions,  $T_0$ , and natural boundary conditions,  $Q_0$ , specified on the surfaces  $\Gamma_u$  and  $\Gamma_q$ , respectively. For nonlinear problems with temperature-dependent material properties, the governing equation is given by

$$\nabla \cdot (\lambda(T) \nabla T) = 0 \quad (2)$$

where  $\lambda(T)$  is the temperature-dependent thermal conductivity. Equation (2) can be linearized by the application of the classical Kirchoff transformation which defines the heat function,  $\Theta$ , as

$$\Theta = \int_0^T \frac{\lambda(T)}{\lambda_0} dT \quad (3)$$

Here,  $\lambda_0$  is a reference conductivity and  $\lambda(T)$  could be an arbitrary function of temperature. Consequently, equation (2) can be transformed into Laplace's equation and solved for the heat function,  $\Theta$ , instead of temperature,  $T$ . Results obtained for the heat function must be transformed back into temperatures using the inverse of the transformation given in equation (3).

Laplace's equation may be solved using the BEM (a weighted residual technique) by introducing an approximation,  $u$ , to the exact solution,  $\Theta$ . Since the approximation is, in general, not equal to the exact solution, an error function or residual is produced in the domain and on the boundary. The residual in the domain is given by  $R = \nabla^2 u$  and the residuals at the boundaries are  $R_u = u - \Theta_0$  and  $R_q = \partial u / \partial n - Q_0$ . These error functions are normally non-zero unless  $u$  is the exact solution. The weighted average of the residual over the domain and on the boundary may be set to zero by the weighted residual statement

$$\int_{\Omega} u^* \nabla^2 u \, d\Omega - \int_{\Gamma_q} (q - Q_0) u^* \, d\Gamma + \int_{\Gamma_u} (u - \Theta_0) q^* \, d\Gamma = 0 \quad (4)$$

where  $u^*$  represents the weight function which is usually called the fundamental solution (Brebbia and Dominguez, 1989), while  $q = \partial u / \partial n$ ,  $q^* = \partial u^* / \partial n$  and  $n$  is the direction of the outward normal to the surface  $\Gamma$ . After integrating by parts twice, the boundary integral equation for Laplace's equation is obtained

$$\int_{\Omega} u \nabla^2 u^* \, d\Omega + \int_{\Gamma} u^* q \, d\Gamma = \int_{\Gamma} q^* u \, d\Gamma \quad (5)$$

The weight function is a Green's function solution for a point-source subject to the homogeneous boundary conditions. For the two-dimensional Laplace's equation it is

$$u^* = \frac{1}{2\pi} \log\left(\frac{1}{r}\right) \quad (6)$$

where  $r = |x_i - x_j|$ ,  $x_i$  is the coordinate of the observation point,  $x_j$  is the coordinate of the source point and the logarithm function here has base  $e$ . The bounding surface  $\Gamma$  is discretized into  $N$  surface elements bounded by  $N$  end-nodes. After discretizing the surface and utilizing the properties of the Dirac delta function, the boundary integral equation (6) can be written as

$$c_i u_i + \sum_{j=1}^{N_{sp}} \int_{\Gamma_j} u q^* \, d\Gamma_j = \sum_{j=1}^{N_{sp}} \int_{\Gamma_j} q u^* \, d\Gamma_j \quad (7)$$

for each  $i$ th node. The term  $c_i$  indicates the scaled internal angle at the  $i$ th surface node. The functions  $u$  and  $q$  are assumed to vary linearly along each surface element and, therefore, they can be defined in terms of their nodal values and interpolation functions

$$u(\xi) = \phi_1(\xi) u_1 + \phi_2(\xi) u_2 \quad \text{and} \quad q(\xi) = \phi_1(\xi) q_1 + \phi_2(\xi) q_2 \quad (8)$$

where  $\xi$  is a localized surface-following dimensionless coordinate, while  $\phi_1 = (1 - \xi)/2$  and  $\phi_2 = (1 + \xi)/2$ . The whole set of equations for the  $N$  nodal values of  $u$  and  $q$  can be expressed in matrix form as

$$[\mathbf{H}] \mathbf{U} = [\mathbf{G}] \mathbf{Q} \quad (9)$$

where  $\mathbf{U} = (U_1, U_2, U_3, \dots, U_N)$  and  $\mathbf{Q} = (Q_1, Q_2, Q_3, \dots, Q_N)$  are vectors containing the nodal potentials and surface panel fluxes while the terms in the  $[\mathbf{H}]$  and  $[\mathbf{G}]$  matrices are assembled by properly adding the contributions from each surface integral

$$H_{ij} = \int_{\Gamma_j} \phi_2 q^* d\Gamma_j + \int_{\Gamma_{j+1}} \phi_1 q^* d\Gamma_{j+1} \quad (10)$$

$$G_{ij} = \int_{\Gamma_j} \phi_2 u^* d\Gamma_j + \int_{\Gamma_{j+1}} \phi_1 u^* d\Gamma_{j+1}$$

The free term,  $q_i$ , is produced when the first surface integral of equation (6) is integrated in the sense of the Cauchy principal value. Since  $q^* = \partial u^* / \partial n = (\partial u^* / \partial r) (\partial r / \partial n) = 0$  when the  $i$ th surface integral contains the  $i$ th observation point, the diagonal of the  $[\mathbf{H}]$  matrix is simply the  $q_i$  term. This coefficient may be computed explicitly by calculating the internal angle at the surface node or implicitly (Brebbia and Dominguez 1989) by first assuming a constant unit potential throughout the entire domain and then solving for the diagonal component as

$$c_i = H_{ii} = - \sum_{j=1}^N H_{ij} \quad i \neq j \quad (11)$$

When the observation node is on the surface panel of integration, the terms in the  $[\mathbf{G}]$  matrix are computed analytically from the integral

$$G_{ii} = \frac{1}{2\pi} \int_{\Gamma_i} \phi_2 \log\left(\frac{1}{r}\right) d\Gamma_i + \frac{1}{2\pi} \int_{\Gamma_{i+1}} \phi_1 \log\left(\frac{1}{r}\right) d\Gamma_{i+1} \quad (12)$$

After the  $[\mathbf{H}]$  and  $[\mathbf{G}]$  matrices are formed, all boundary conditions are applied and a set of linear algebraic equations,  $[\mathbf{A}] \mathbf{X} = \mathbf{F}$ , is constructed. Known or specified surface potentials,  $U_j$ , and fluxes,  $Q_j$ , are assembled on the right-hand-side of the equation set and are multiplied by their respective  $[\mathbf{H}]$  or  $[\mathbf{G}]$  matrix row thus forming the vector of knowns,  $\mathbf{F}$ . All unknown potentials or fluxes are assembled on the left-hand-side of the equation set and are represented by a coefficient matrix  $[\mathbf{A}]$  multiplying a vector of unknown quantities,  $\mathbf{X}$ .

The set of linear algebraic equations is then solved for the unknown surface potentials,  $U$ , and fluxes,  $Q$ , using a singular value decomposition (SVD) matrix solver (Press et al. 1992). We used the SVD since the matrix tends to become ill-conditioned or singular (several equations become linearly dependent with other equations in the equation set) whenever the over-specified thermal data are farther away from the surfaces where no boundary conditions are applied. If

additional thermal data within the solid is provided, additional equations may be added to the equation set. Note that the SVD algorithm is capable of providing a satisfactory solution vector even when the [A] matrix is not square. The more rows (i.e. more data points) that are provided to the system, the more accurate the solution vector becomes, although the reverse is true when the matrix has less rows than columns. Once the matrix is solved, the entire thermal field within the solid can be easily deduced.

## RESULTS AND DISCUSSION

### IHCP for a Square Plate Using the BEM

A BEM computer program was developed using the theory discussed in the previous section. The accuracy of the BEM as a solution to the IHCP was verified for a solid square plate. The plate was 6.0 m on each side and the thermal conductivity of the plate was chosen as 1.0 W/mK. The top and bottom boundaries were specified to be adiabatic ( $Q_0 = 0 \text{ W/m}^2$ ) while the left side surface of the plate was over-specified with a temperature boundary condition of  $T_0 = 300 \text{ K}$  and a heat flux boundary condition of  $Q_0 = -50 \text{ W/m}^2$ . The right side boundary was considered to be inaccessible and, as such, both temperature and heat flux were unknown on this boundary. The plate boundary was discretized with 12 panels (3 per each of the four sides) on the boundary of the solid. The BEM was successful in computing a temperature field within the plate that was accurate to almost the floating point precision of the computer. The computed temperature and heat flux on the right side boundary were 0.000161 K and 49.99997 W/m<sup>2</sup>, respectively.

### Study of the IHCP for an Annular Disk Using the BEM

The behavior of this algorithm for various combinations of boundary conditions was documented for steady-state heat conduction in an annular solid disk. The outer radius of the disk was 1.2 in and the centrally located hole had a radius of 0.5 in. The analytic solution for this problem was developed by applying Dirichlet or essential boundary conditions everywhere on the boundary of the annular region. Temperature boundary conditions of 100°C on the outer boundary and 50°C on the inner boundary were enforced. The thermal conductivity of the solid was considered to be constant,  $\lambda = 1.0 \text{ Btu/in sec}^\circ\text{R}$ . The analytic solution for the temperature field within the disk is easily found as

$$T(r) = A + B \log r \quad (13)$$

where  $A = 89.59$  and  $B = 57.11$ . The radial heat flux is then

$$Q(r) = -\lambda \nabla T = -\lambda dT(r)/dr = B / r \quad (14)$$

which yields  $Q_{\text{out}} = -47.59 \text{ Btu/in}^2\text{sec}$  and  $Q_{\text{in}} = 114.22 \text{ Btu/in}^2\text{sec}$  as heat fluxes through the outer and inner boundaries, respectively. The BEM algorithm was run on the same problem. The problem was discretized with 36 panels on each outer and inner boundary. The BEM program predicted the temperature field in the solid which averaged only a 0.3% error versus the analytic solution.

In order to study the feasibility and accuracy of the BEM solution to the steady-state IHCP, seven variations to the same problem were performed and the results obtained were compared to those from the previous problem. Each test utilized the same annular geometry and outer boundary thermal data in a variety of combinations.

Test 1. The outer and inner boundaries of the annular domain were each discretized with 36 equally-length flat panels. The entire outer boundary was over-specified with temperature and flux boundary conditions, while both temperature and flux were unknown on the inner boundary. The

BEM formulation detailed in the theory section, can be represented in matrix form by equation (9). For this test case, the solution set of 72 equations included 72 known values given as boundary conditions on the outer surface and 72 unknowns on the inner boundary. The BEM computed the temperature field within the annular solid in addition to the unknown temperatures and heat fluxes on the inner boundary. Figure 2a shows the computed temperature contours for the annular solid disk and also includes the BEM nodes used and the type of boundary conditions specified at each node. The box-shaped nodes have both T and Q known and thus are over-specified, the circles are nodes where both T and Q are unknown, and the triangular nodes have a single boundary condition of temperature applied. The thick solid lines in figures 3 and 4 represent the accuracy of this particular BEM solution. Figure 3 shows the relative percentage error in temperature on the inner boundary for each test as a function of the circumferential angle in radians. Figure 4 is the same as figure 3 except that it gives the relative percentage error in the heat flux on the inner boundary. Notice that this test case had an almost perfectly symmetric result with an average error of only 0.5% in temperature and a somewhat oscillating error in heat flux averaging about -1.5%.

Test 2. This test case was identical to Test 1 except that the outer and inner boundaries were discretized with a coarser grid consisting of 18 panels each. Overall, the BEM solution set had 36 knowns, 36 unknowns and 36 equations. The computed temperature field and boundary discretization are shown in Figure 2b and the relative percentage error in temperature and heat flux on the inner boundary are given as thin solid lines in figures 3 and 4. The temperature field within the solid was nearly perfectly symmetric, but was uniformly biased about 2.5% in temperature and -2.5% in heat flux.

Test 3. This test case was identical to Test 1 except that the boundary of the annular disk was discretized with 36 panels on the outer boundary and 18 panels on the inner boundary. Overall, the BEM solution set was over-specified and had 72 knowns, 36 unknowns and 54 equations. The thick dotted lines in figures 3 and 4 readily show that Test 3 produced the most accurate results for both temperature and heat flux. In addition, the temperature contours in Figure 2c are nearly perfectly symmetric.

Test 4. This test was identical to Test 1 except that the outer boundary was discretized with 18 panels and the inner boundary was discretized with 36 panels. Overall, the BEM solution set was under-specified and had 36 knowns, 72 unknowns and 54 equations. Results of Test 4 are given by the thin dotted line in figures 3 and 4. The temperature was uniformly biased with a 3.0% error, while the heat flux was somewhat oscillatory and similarly biased. The temperature contours in figure 2d were nearly symmetric.

Test 5. Both the outer and inner boundaries of the annular disk were discretized with 36 panels. Temperature boundary conditions were specified everywhere on the outer boundary but the additional heat flux boundary conditions were over-specified in the first and third quadrants of the outer boundary only. The BEM solution set had 54 knowns, 90 unknowns and 72 equations. The temperature field shown in figure 2e was comparable to that of Test 4. The temperature and heat flux on the inner boundary are represented by the finely dotted lines. The temperature distribution on the inner boundary was somewhat oscillatory, but averaged only a 0.75% error. The heat flux on the inner boundary was also oscillatory and averaged an error of about -2.0%.

Test 6. The circular disk was discretized with 36 panels on both the inner and outer boundaries. Temperature boundary conditions were specified on the entire outer boundary, while heat flux boundary conditions were over-specified only on the upper half of the outer boundary. As in Test 5, the BEM solution set contained 54 unknowns, 90 unknowns and 72 equations. The temperature field illustrated in figure 2f was asymmetric about the x-axis, but was very nearly symmetric about the y-axis. The greatest error in the temperature field occurred in the bottom half of the annular solid region. The thick dashed lines in figures 3 and 4 reveal inner boundary errors that are quite oscillatory in nature and noticeably peak at the very bottom of the solid disk (the point farthest from the over-specified data).

Test 7. This test case is identical to Test 5, except that heat flux boundary conditions are over-specified in the first quadrant of the outer boundary only. The BEM solution set contained 45 knowns, 99 unknowns and 72 equations. Figure 2g illustrates the temperature contours within the solid disk. The error in the temperature field obviously worsens as the distance from the over-

specified data increases. The thin dashed lines in Figures 3 and 4 illustrate the error in the temperature and heat flux on the inner boundary. The error is oscillatory and peaks at about 60% at the point farthest from the over-specified data. Notice also that the temperature field is symmetric about the line inclined 45 degrees and passing through the center of the circle.

### IHCP for a Rocket Nozzle Wall Section with a Coolant Flow Passage

The BEM solution to the IHCP was attempted on a realistic engineering problem with temperature-dependent material properties. High pressure, reusable rocket thrust chambers encounter a progressive thinning of the coolant flow passage wall after repetitive engine operation. This deformation is caused by high thermal plastic strains that eventually cause cracks to form in the cooling passage wall. An engineer who wishes to reduce or eliminate the plastic strain may obtain experimental data such as hot gas wall temperatures and heat fluxes, shroud temperatures, compressive strains, and thrust chamber total pressure and temperature (Quentmeyer 1978, 1992). Unfortunately, the engineer cannot normally obtain data within the coolant flow passage due to the extremely low temperature of the liquid hydrogen coolant and the small dimensions of the passage.

Figure 5 is a schematic of a cylindrical thrust chamber assembly and figure 6 illustrates a cylinder wall cross section showing typical instrumentation locations and dimensions. These figures were taken from a NASA publication (Quentmeyer 1978) and were subsequently used to generate the geometry of the nozzle wall section. The hot gas wall temperature (1520 °R), heat flux (-35 Btu/in<sup>2</sup>sec) and shroud temperature (518.4 °R) were experimental measurements taken from the same publication. The outer shroud heat flux was assumed to be negligible (0 Btu/in<sup>2</sup>sec). The coefficient of thermal conductivity of the solid copper region was linearly dependent on the local temperature

$$\lambda = \lambda_0 ( 1 + \alpha T ) \quad (15)$$

where  $\lambda_0 = 0.004893 \text{ Btu/insec}^\circ\text{R}$  and  $\alpha = -0.000055056 \text{ }^\circ\text{R}^{-1}$ . In addition, figure 6 shows that the conducting solid region is made up of three different materials; copper, electrodeposited copper, and nichrome ZrO<sub>2</sub>. Although the present analysis uses only a single material, the BEM can be modified to handle composite materials with each having distinct thermal properties. The shaded portion in figure 6 is the domain typically used in the two-dimensional heat conduction model. For the BEM analysis of this IHCP, a full section containing the entire cooling passage and half of the surrounding conducting metal was generated in order to examine the symmetry of the results. The meridional or symmetry planes were assumed to be adiabatic. The outer and inner boundaries were discretized in the same manner: 16 panels on the hot gas side, 8 panels on the shroud and 8 panels on each of the two periodic meridional boundaries. The BEM solution set contained 66 knowns, 94 unknowns and 80 equations. The BEM computed both temperatures and heat fluxes on the entire coolant flow passage boundary in addition to the temperatures on the meridional side boundaries. The predicted temperature field within the solid region is illustrated in figure 7. These results show a negligible asymmetry about the meridional centerline and slight oscillations in the temperatures computed near the corners of the coolant passage's cool side.

### CONCLUSIONS

The boundary element method computed temperature and heat flux boundary conditions on boundaries of a conducting solid where such quantities were originally inaccessible and unknown. The results presented herein indicate that the direct non-iterative BEM solution method for the IHCP is an accurate, robust and reliable technique that takes only seconds of CPU time on any typical mainframe, workstation or PC. In addition, the results obtained were found to be more accurate when one or both of the following conditions were observed: a) greater amount of over-

specified data was applied, b) the over-specified data locations were in close geometric proximity to the locations of the unknown boundary conditions.

## ACKNOWLEDGEMENTS

Sincere thanks are due Mr. Vineet Ahuja for suggesting the use of the SVD algorithm for almost singular matrices, since a standard matrix solver produced meaningless results due to severe accumulation of round-off errors.

## REFERENCES

- Beck, J.V., Blackwell, B. and St. Clair, C.R., Jr.: *Inverse Heat Conduction: Ill-Posed Problems*. Wiley-Interscience, New York, 1985.
- Brebbia, C.A. and Dominguez, J.: *Boundary Elements, An Introductory Course*. McGraw-Hill Book Company, New York, 1989.
- Hensel, E.C., Jr.: *Multi-dimensional Inverse Heat Conduction*. Ph.D. dissertation, Mechanical Engineering Dept., New Mexico State University, Las Cruces, NM, 1986.
- Hills, R.G. and Hensel, E.C., Jr.: *One-dimensional Nonlinear Inverse Heat Conduction Technique*. *Numerical Heat Transfer*, vol. 10, pp. 369-393, 1986.
- Martin, T.J.: *Inverse Design and Optimization of Two- and Three-Dimensional Coolant Flow Passages*. M.S. Thesis, Dept. of Aerospace Engineering, The Pennsylvania State University, May 1993.
- Murio, D.A.: *The Mollification Method and the Numerical Solution of Ill-Posed Problems*. John Wiley & Sons, Inc., New York, 1993.
- Press, W.H., Teukolsky, S.A., Vetterling, W.T. and Flannery, B.P.: *Numerical Recipes in FORTRAN*. Second Edition, Cambridge University Press, 1992.
- Quentmeyer, R.J.: *Investigation of the Effect of Ceramic Coatings on Rocket Thrust Chamber Life*. NASA TM-78892, 1978.
- Quentmeyer, R.J.: *An Experimental Investigation of High-Aspect-Ratio Cooling Passages*. NASA TM-105679, 1992.
- Stolz, G. Jr.: *Numerical Solutions to an Inverse Problem of Heat Conduction for Simple Shapes*. *ASME Journal of Heat Transfer*, vol. 82, pp. 20-26, 1960.

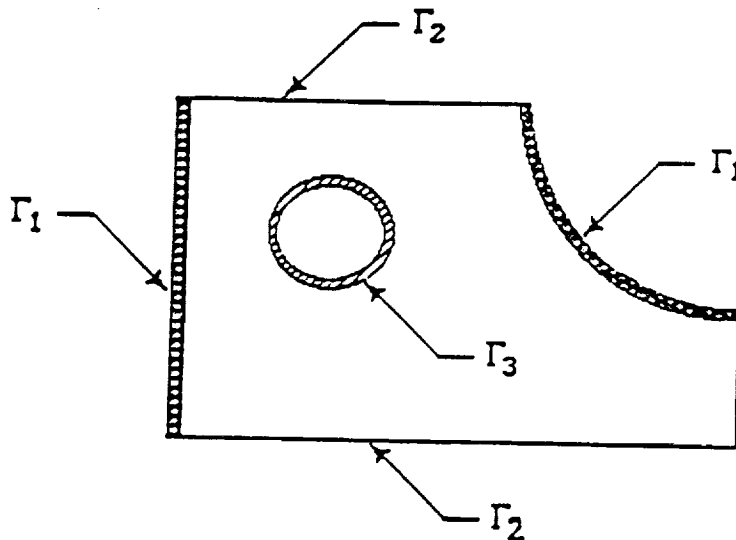
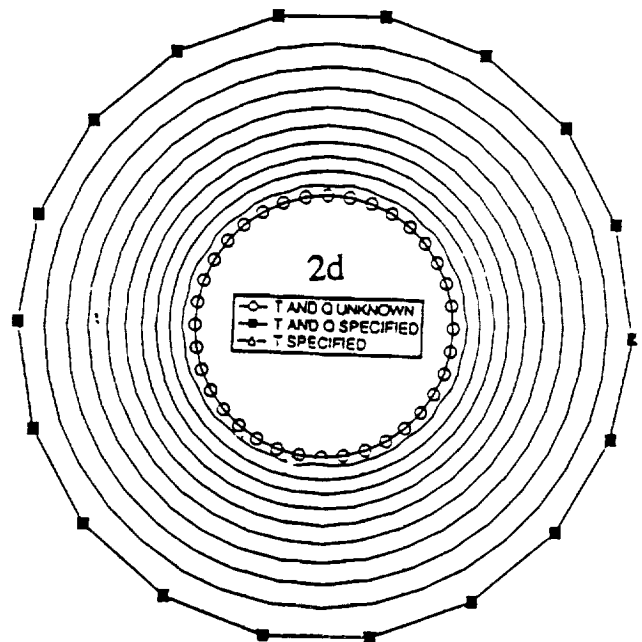
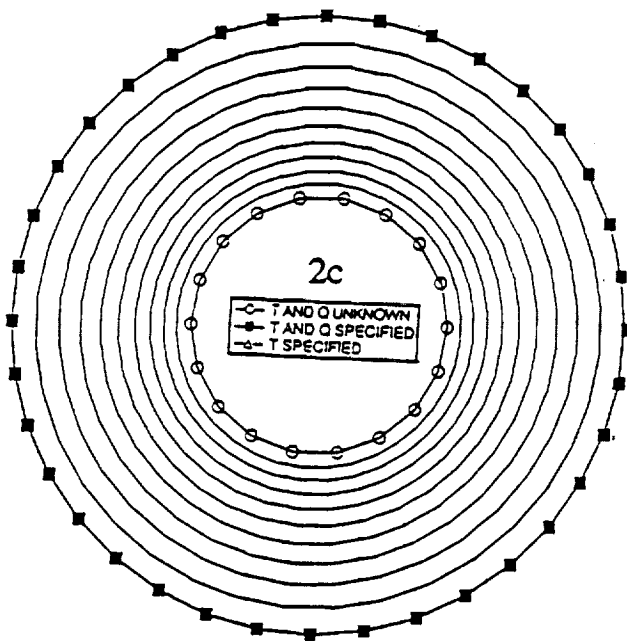
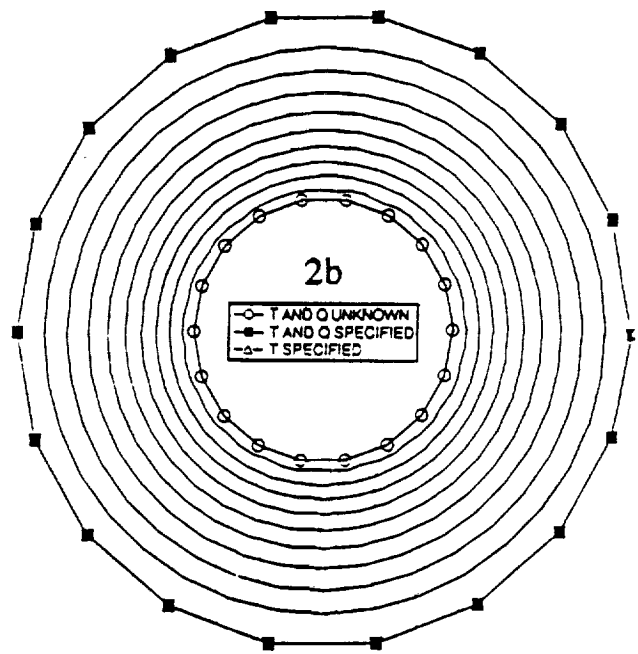
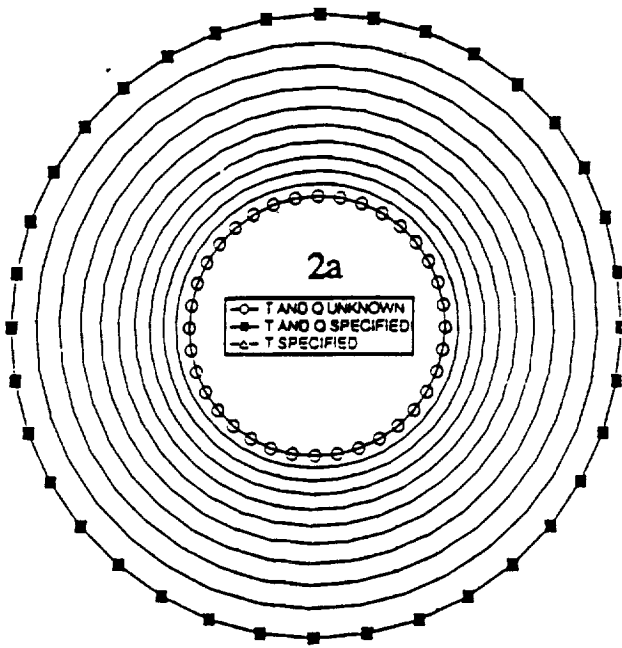


Figure 1. A geometric definition of a two-dimensional inverse heat conduction problem.



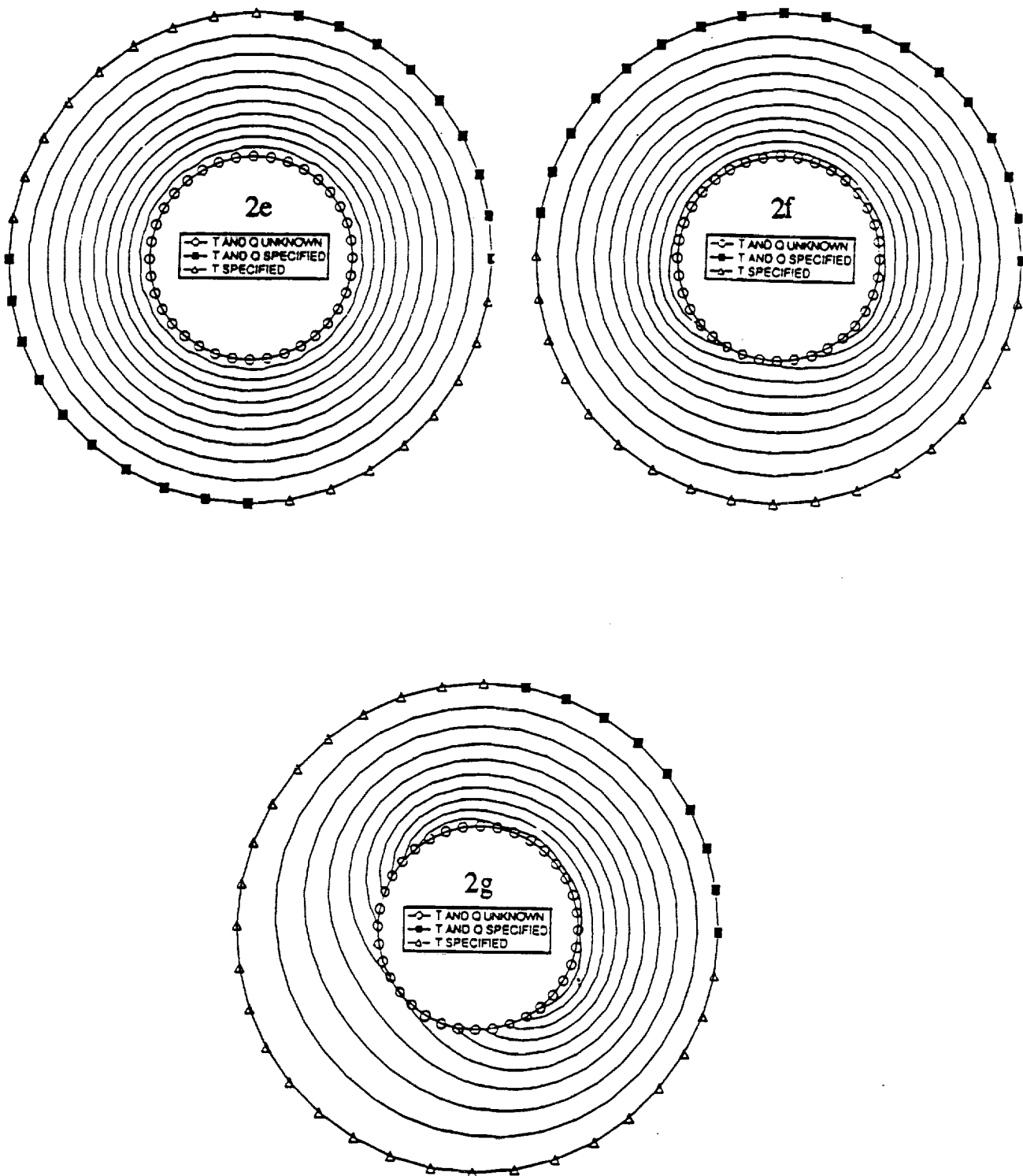


Figure 2. Geometry of the BEM nodes on the outer and inner boundaries, boundary condition types and isotherms computed with the BEM for each of the seven annular disk test cases.

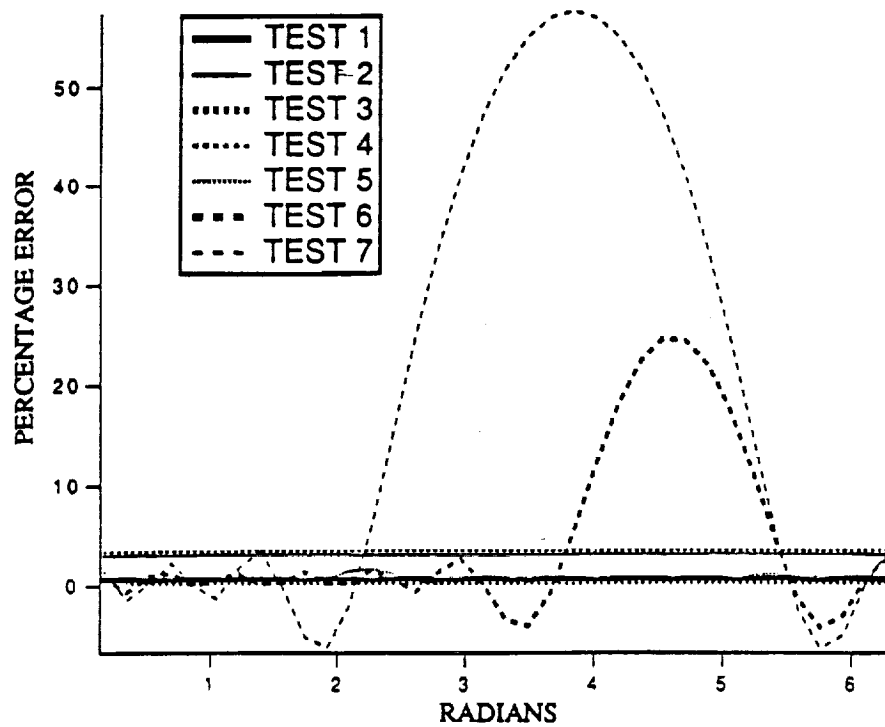


Figure 3. Relative percentage errors (BEM versus analytic solution) of the inner boundary temperatures for each of the seven annular disk test cases.

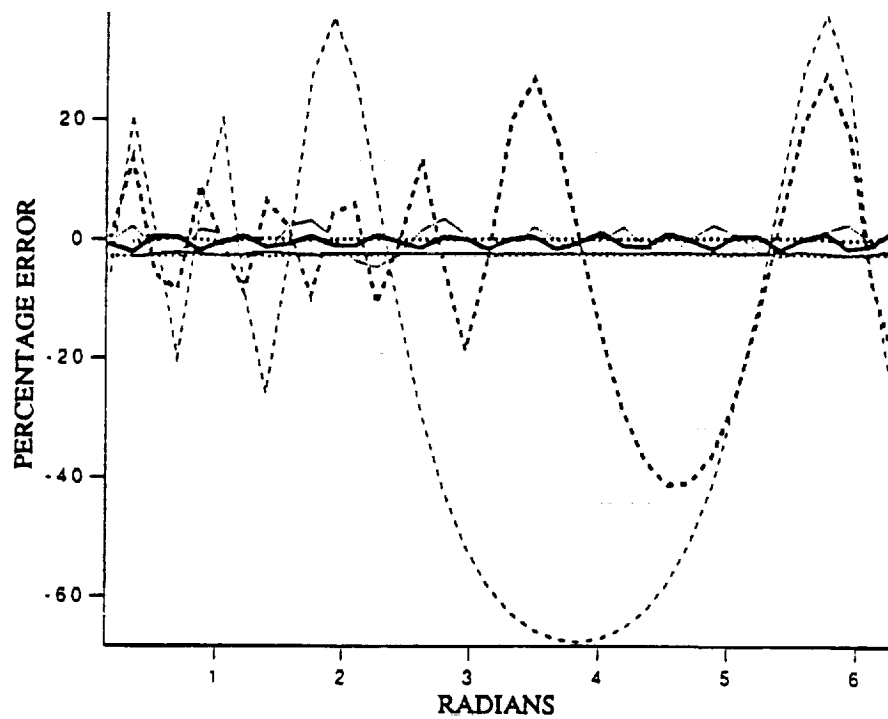


Figure 4. Relative percentage errors (BEM versus analytic solution) of the inner boundary heat fluxes for each of the seven annular disk test cases.

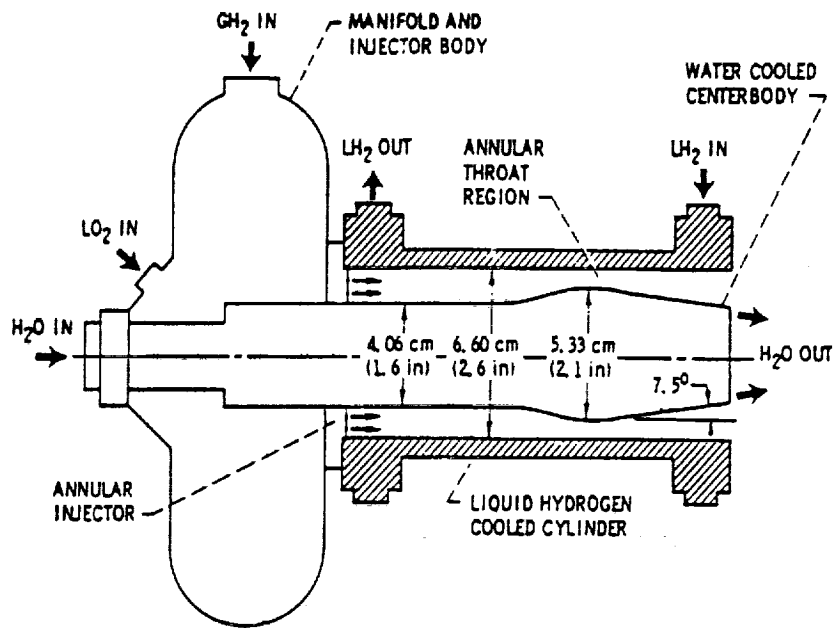


Figure 5. Schematic of cylindrical thrust chamber assembly (Quentmeyer 1978).

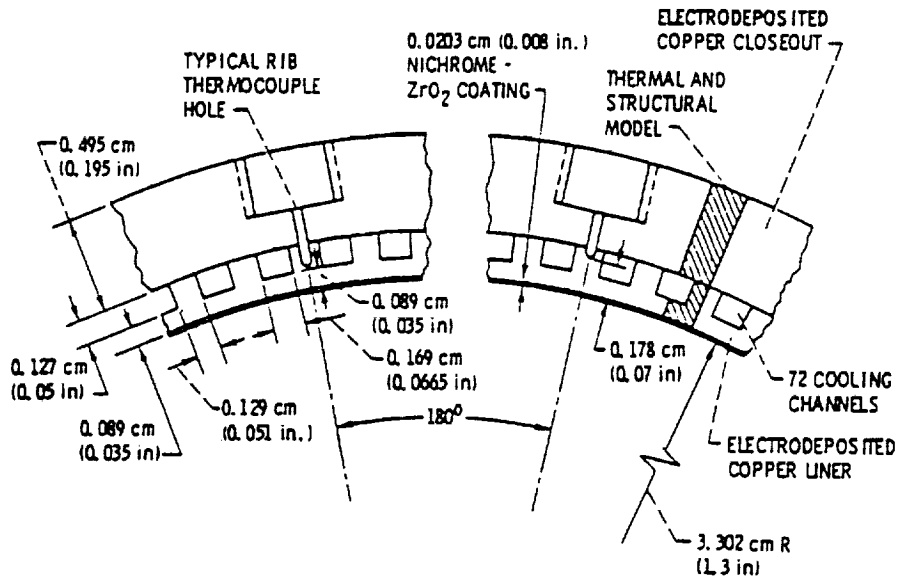


Figure 6. Cylinder wall cross section showing instrumentation locations and dimensions (Quentmeyer 1978).

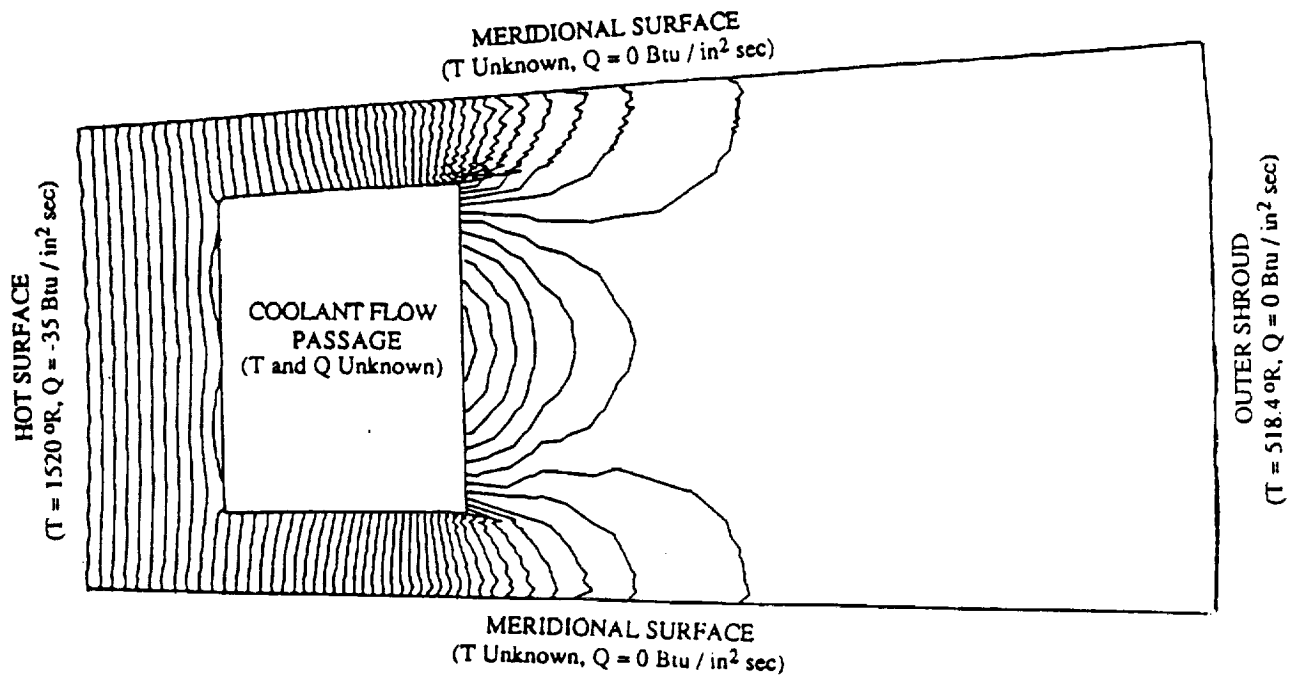


Figure 7. Geometry, boundary conditions and isotherms computed using the BEM for a two-dimensional section of a thrust chamber wall with a coolant flow passage.

